Environmental Pollution 237 (2018) 968–976

Contents lists available at ScienceDirect

Environmental Pollution

journal homepage: www.elsevier.com/locate/envpol

In-situ examination of graphene and graphene oxide impact on the depuration of phenanthrene and fluoranthene adsorbed onto spinach (*Spinacia oleracea* L.) leaf surfaces☆

Haifeng Sun [a, b], Ruijie Feng [a], Yanli Nan [a], Zhang Chen [c], Nan Sang [a, *]

[a] College of Environment and Resource, Shanxi University, Taiyuan 030006, China
[b] Guangzhou Key Laboratory of Environmental Exposure and Health, School of Environment, Jinan University, Guangzhou 510632, China
[c] Institute of Loess Plateau, Shanxi University, Taiyuan 030006, China

ARTICLE INFO

Article history:
Received 11 July 2017
Received in revised form
1 November 2017
Accepted 2 November 2017
Available online 11 November 2017

Keywords:
In situ
Polycyclic aromatic hydrocarbons
Graphene
Graphene oxide
Depuration

ABSTRACT

To further assess the human being's exposure to polycyclic aromatic hydrocarbons (PAHs) through the dietary pathway, understanding the partitioning of these chemicals co-existed with nanomaterials in edible vegetable systems deserves specific consideration. In this study, the fiber-optic fluorimetry was applied to *in situ* examine the effects of graphene (GNS) and graphene oxide (GO) nanosheets on the quantification and depuration of three-ringed phenanthrene (Phe) and four-ringed fluoranthene (Fla) adsorbed individually onto the living spinach (*Spinacia oleracea* L.) surfaces. When the GNS and GO dosages separately increased to the maximum values: a respective red-shift of 4–5 nm and blue-shift of 2–3 nm occurred for the optimal detection emission wavelengths (λ_{em}) of the two PAHs, indicating that individual GNS and GO resulted in different changes to the epicuticular wax (ECW) polarity; GNS-inducing fluorescence quenching for the PAHs was about two times greater than GO, owing to the stronger π-π interactions between PAH molecules and GNS relative to GO; the volatilization coefficients (k_{C1}) were reduced by 31.1% versus 26.7% for Phe, and 51.6% versus 34.4% for Fla, mainly via providing an additional adsorbent and promoting the accessibility of the leaf cuticle; respective photolysis coefficients (k_{P2}) of Phe and Fla decreased by 42.9% and 50.0% with GNS, primarily owing to the enhancement of the ECW light-adsorption capacity, but increased by 33.3% and 40.0% with GO due to its photocatalytic activities; overall, total depuration coefficients (k_{T1}, k_{T2}) of the two PAHs decreased by 11.1–55.6%. These findings demonstrate that GNS and GO significantly alter the depuration behavior of PAHs in vegetable systems, potentially posing a threat to the safety of edible vegetables.

1. Introduction

Polycyclic aromatic hydrocarbons (PAHs) are known to be widespread hazardous pollutants produced via natural and anthropogenic sources, generated during the incomplete combustion of solid and liquid fuels or derived from industrial activities (Wang et al., 2014b; Andersson and Achten, 2015). Due to the high degree of mutagenicity and carcinogenicity, some atmospheric PAHs are harmful to mammals and human health through inhalation, ingestion and dermal contact (Sun et al., 2016a). Generally, the outer surfaces of vegetation are hydrophobic environments that can enrich hydrophobic PAHs mainly from the atmosphere (Li et al., 2009; Li and Chen, 2009). Therefore, the transfer of PAHs between the air and vegetation surfaces has been reported to play an important role in influencing atmospheric concentrations, regional/global cycling and public health hazard (Nizzetto et al., 2014). As primary food producers, edible vegetables constitute a direct exposure pathway to human health. Clearly, extensive studies on the environmental behavior of PAHs between the air and vegetable surfaces have significant implications to fully understand the impact of PAH chemicals on the vegetable safety and risk assessments.

To date, numerous studies have been conducted to investigate the disappearance of PAHs adsorbed onto the cuticle surface of vegetation, including pine needles (Wang et al., 2005), mangrove species (Sun et al., 2013a), and crop species (Sun et al., 2016b), and

☆ This paper has been recommended for acceptance by B. Nowack.
* Corresponding author.
E-mail address: sangnan@sxu.edu.cn (N. Sang).

https://doi.org/10.1016/j.envpol.2017.11.007
0269-7491/

the depuration of adsorbed PAHs is mainly caused by volatilization and photolysis. In our recent study, the effects of two surfactants, namely, polyoxyethyleneglycol dodecyl ether (Brij35) and sodium dodecylbenzene sulfonate (SDBS), on the depuration of PAHs adsorbed onto the living soybean leaf surfaces were determined *in situ*, and the total depuration rates of the PAHs increased by 10.1–27.1% with the presence of Brij35, while decreased by 23.2–30.5% with SDBS (Sun et al., 2016b). However, limited studies have been focused on how some of the emerging environmental factors affect the depuration of adsorbed PAHs from the leaf surface of edible vegetable.

The development and utilization of engineered nanomaterials (ENMs) have increased significantly over the last few decades. Statistically, more than 1300 nano-enhanced products are commercially available, including electronics, textiles, food packaging, sunscreens and personal care products, and a multitude of other products (De La Torre-Roche et al., 2013; Mitrano et al., 2015). Currently, the extended application of nanotechnology in crop and vegetable improvement is being explored and utilized, ranging from nanoemulsions to preservatives in fertilizer/pesticide to production improvement technologies and modified plastic packaging for vegetable commodities (Peralta-Videa et al., 2011; Trujillo-Cayado et al., 2017). There have been several studies concerning the interaction of nanomaterials with organic contaminants (Wang et al., 2015) and other chemical constituents (pesticides, fertilizers) in agroecosystems, since their co-existence may represent a significant and uncharacterized pathway to human exposure. Corredor et al. (2009) reported that carbon-coated Fe nanoparticles serving as carrier agents could deliver chemicals into specific plant tissues. Similarly, the occurrence of fullerene exposure significantly increased the accumulation capacity of *p, p′*-DDE in the root and whole plant body of zucchini, soybean and tomato, and enhanced the contaminant uptake ranging from 30 to 65% (De La Torre-Roche et al., 2012). Recently, Zhang et al. (2017) investigated the phytotoxicity, uptake and transformation of nano-CeO_2 in sand-cultured romaine lettuce. However, there has been little research concerning the effects of ENMs on the depuration of PAHs adsorbed onto vegetable leaf surfaces.

As a member of the carbonaceous nanomaterials, Graphene (GNS) is characterized as a 2D monolayer of sp^2-hybridized carbon atoms that are packed in a hexagonal honeycomb lattice (Geim and Novoselov, 2007; Yu et al., 2015), and constitutes the basic structure unit of the carbon nanotube. Additionally, the oxygen-containing functional groups cause graphene oxide (GO) to be hydrophilic by interrupting the sp^2-hybridized structure. As is well known, their available spaces providing the interaction with organic contaminants are mainly dependent on their monomer conformation. Recently, GNS has been reported to exhibit excellent performance in adsorbing some organic contaminants, including pesticides (Maliyekkal et al., 2013), PAHs (Wang et al., 2016), phenolic compounds (Yu et al., 2017). For instance, Wang et al. (2014b) determined the potential adsorptive sites of naphthalene (Nap), phenanthrene (Phe) and pyrene (Pyr) onto GNS and GO nanosheets and related molecular mechanisms. However, there is still a lack of knowledge in regard to the effects of GNS and GO on the environmental behavior of PAHs in vegetable species.

In this work, *Spinacia oleracea* L. was chosen for the study since spinach is among the most common vegetable that is consumed around the world. Phe and fluoranthene (Fla) were selected as the model components of three- and four-ringed PAHs, respectively, due to their abundance in both spinach leaves and the gas phase (Khillare et al., 2012; Sun et al., 2016a). The objective of the current study was to *in situ* examine the impact of GNS and GO on the depuration of Phe and Fla adsorbed onto the living spinach leaf surfaces using the fiber-optic fluorimetry.

2. Materials and methods

2.1. Apparatus and reagents

GNS (98% purity, thickness: 0.55–3.74 nm, diameter: 0.5–3 μm, layers: < 10, Alfa Aesar) and GO (99% purity, thickness: 0.55–1.2 nm, diameter: 0.5–3 μm, layers: < 3, Alfa Aesar) were acquired from Accelerating Scientific and Industrial Development thereby Serving Humanity, Beijing, China. The structures of GNS and GO were characterized using Raman spectra (Fig. S1). The surface functional groups were observed by Fourier transform infrared spectroscopy (FTIR) (Fig. S2) and X-ray photoelectron spectroscopy (XPS) (Figs. S3a and b). The detailed discussion is presented in Supporting Information (SI). GNS and GO suspensions dispersed in water with the same concentration of 1000 mg L^{-1} were prepared, and were sonicated for 10 min, followed by incubation on the bench overnight. The aqueous dispersions of GNS and GO were monitored by the zeta potential (Mueller et al., 2010) and the results are represented in Fig. S4. When the pH was higher than 6, the zeta potentials of GNS and GO were both smaller than minus 45 mV, indicating the ideal values for stabilizing colloidal particles.

The method details for preparing stock working solutions of Phe and Fla (purity > 99%, Sigma, USA) was recorded in SI. The samples (PAH solutions with GNS or GO) were prepared by mixing their stock solutions in setting points first and then the mixing solutions were diluted, whereas the controls (PAH solutions without GNS or GO) were obtained by diluting solute stock solutions alone. All of the other chemicals (A.R.) used in this study were obtained from Shanghai Trustin Chemical Co., Ltd (China).

2.2. Depuration experiment

The way for cultivation, selection and pretreatment of spinach seedlings has been displayed in SI. Six groups of spinach seedlings were chosen, and each group with equal numbers was treated differently, and in total, there were six types of treatments: 1. Phe alone; 2. Phe + GNS; 3. Phe + GO; 4. Fla alone; 5. Fla + GNS; 6. Fla + GO. For each treatment, five replicate plants and five replicate leaves (one per plant) were selected for the depuration experiment. With the help of a 10-μL flat head micro-injector (Shanghai Medical Laser Instrument Plant, China), each sample and control mentioned in section 2.1 was evenly introduced onto the corresponding 'spot' with area of approximately 0.28 cm^2 that was used as the detection location. The making method of the 'spot' is shown in SI.

In this study, the spinach plants with their leaves contaminated by PAHs were evenly split into two sets. One group of plants was exposed to solar irradiation in Shanxi University (N 37°46′, E112°38′), Taiyuan, China, from 9.00 a.m. to 5.00 p.m., in September 2016 under clear skies, which referred to as the light group. Within the 72-h period of depuration experiment, local solar irradiation intensity varied between 60 and 890 W m^{-2}, a daily mean temperature ranged from 20 to 29 °C, and mean relative humidity was 38 ± 3%. The other group of plants was transferred to a dark room to protect them from solar irradiation, which referred to as the dark control in this study. During the experiments, all of the atmospheric conditions provided for the controls kept basically consistent with those for the light-treated plants. Normally, the relative humidity and temperature of the controls differed by < 2 °C and 2% from those with solar irradiation, respectively. The objective of the control group was to determine the impact of the GNS and GO on the volatilization of adsorbed PAH chemicals, while providing full sunlight irradiation aimed to evaluate the effects of GNS and GO on both volatilization and photolysis.

2.3. Measurement of PAHs sorbed on the vegetable leaf surfaces

A Cary Eclipse fluorescence spectrophotometer equipped with fiber optic accessories with the length of 2 m (Agilent, California) (Fig. 1) was used to obtain the fluorescence spectra of Phe and Fla adsorbed onto the living spinach leaf surfaces, and the established fiber-optic fluorimetry was suitable for the *in situ* quantification of the two adsorbed PAHs. The experimental procedures were displayed in SI. The key instrumental parameters were shown as follows: excitation and emission slits were both fixed at 10 nm; scan speed was fixed at 12,000 nm min^{-1}. Detailed operations were the same as those recorded in the reference (Chen et al., 2010). To further verify the suitability of the fiber-optic fluorimetry, the amount of PAHs in leaf samples were determined using a Hewlett-Packard 5890 gas chromatograph (GC) equipped with DB-5 (30 m × 0.25 mm × 0.25 μm Film) coupled to a HP 5972 mass spectrometer (MS). The specific operations referred to the method reported by Smith et al. (2001), and more details were shown in SI.

2.4. Quality assurance and quality control

Based on our reported method (Sun et al., 2016b), the interference and recovery experiments were performed to verify the accuracy and precision of the available analytical approach. For a fixed concentration of Phe or Fla, the variation of GNS and GO dosages had no significant effects on the detected amount of PAHs on the spinach leaf surfaces (Table S1). Recoveries for the Phe and Fla were in the range of 89.6–104.4% and 85.4–103.8%, respectively (Table S2). In addition, the relative standard deviation (RSD) for the *in situ* determination of adsorbed Phe and Fla were in the range of 4.6–8.2% and 5.1–9.4%. These results confirmed that the accuracy and precision of the fiber-optic fluorimetry was acceptable.

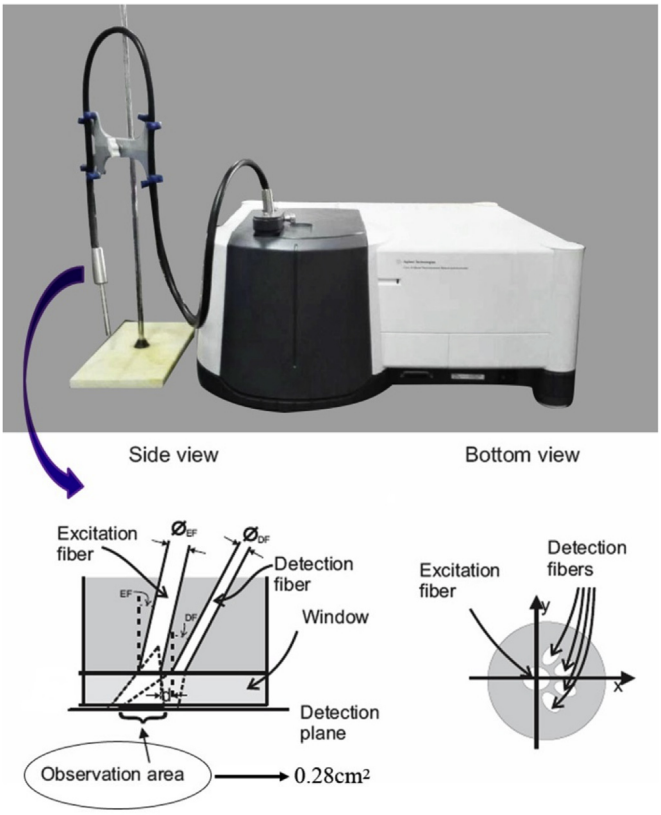

Fig. 1. Schematic diagram of the determination device and fiber-optic accessories.

For every item, the average value of nine measurements was presented as the final results. All differences of statistical significance among treatments were determined using one-way analysis of variance (ANOVA) tests followed by the Student-Newman-Keuls (SNK) Multiple Comparison Test ($p < 0.05$). All statistical analysis was handled using SPSS 13.0.

3. Results and discussion

3.1. Effects of GNS and GO on the fluorescence spectra of PAHs adsorbed onto the spinach leaf surfaces

First, the fluorescence emissions were optimized for Phe and Fla adsorbed onto the spinach leaf surfaces by determining the effect of GNS and GO on the fluorescence emission spectrum of the two PAHs. With GNS and GO of inclusion or exclusion, the fluorescence emission spectra of Phe and Fla adsorbed singly at a concentration of 400 ng $spot^{-1}$ was acquired separately (Fig. S5). Without the GNS and GO nanosheets, the optimal excitation (λ_{ex}) and emission wavelength (λ_{em}) were located at 255 nm and 370 nm for the *in situ* measurement of Phe, and 359 nm and 466 nm for Fla. Statistically, with the increasing GNS and GO concentrations, a significant red-shift and blue-shift occurred for λ_{em}, respectively ($p < 0.05$) (Fig. S5). In detail, a red shift of 4–5 nm was yielded when the GNS dosages increased up to 600 ng $spot^{-1}$, indicating probably a decrease in the polarity of the leaf epicuticular wax (ECW), while a blue shift of 2–3 nm occurred as GO concentration increased up to 500 ng $spot^{-1}$, suggesting an increase in the polarity of ECW. These observations showed that the two types of nanosheets brought different effects to the microenvironment of the spinach leaf surfaces.

To address the impact of the two types of nanosheets on the relative fluorescence intensity (RFI) of the two adsorbed PAHs, the RFI of Phe and Fla at the same concentration of 400 ng $spot^{-1}$ was obtained at the optimal emission wavelength by varying GNS and GO concentrations from 100 to 600 ng $spot^{-1}$, and then the Phe and Fla concentrations were separately varied from 50 to 800 ng $spot^{-1}$ with GNS and GO at a concentration of 300 ng $spot^{-1}$. From Fig. 2, the fluorescence intensity of the two selected PAHs decreased rapidly initially with a separate increase in the GNS and GO concentrations to 300 ng $spot^{-1}$ and 200 ng $spot^{-1}$, and then decreased at a decreasing rate when reaching higher concentrations. Nevertheless, within a certain range, RFI (y) was positively correlated with the PAH concentrations (x) with or without GNS and GO, which was addressed by taking GNS and GO with the respective concentrations of 300 ng $spot^{-1}$ and 200 ng $spot^{-1}$ as examples in this study (Fig. 2). The excellent linear relationship between RFI and the PAH concentrations clearly demonstrates the availability of the analytical method in directly quantifying the amount of PAHs adsorbed individually onto the leaf surfaces of living spinach seedlings, and the analytical merits, including the calibration curve, linear range, correlation coefficient and detection limit, are displayed in Table 1. In the absence of GNS or GO, the detection limits for the *in situ* determination of Phe and Fla adsorbed onto the spinach leaf surfaces were 2.3 ng $spot^{-1}$ and 1.2 ng $spot^{-1}$, respectively (Table 1). In our previous studies, the fiber-optic fluorimetry has been developed for the *in situ* quantification of the PAHs adsorbed onto the leaf surfaces of living mangrove (Chen et al., 2010) and crop seedlings (Sun et al., 2016a), and the detection limits for the *in situ* quantification of Phe and Fla ranged from 0.9 to 2.7 ng $spot^{-1}$. Therefore, the observation in this study was comparable to our previously reported results.

Furthermore, the detection sensitivities of the analytical method for the *in situ* measurement of the two adsorbed PAHs decreased when GNS or GO nanoparticles were present (Table 1).

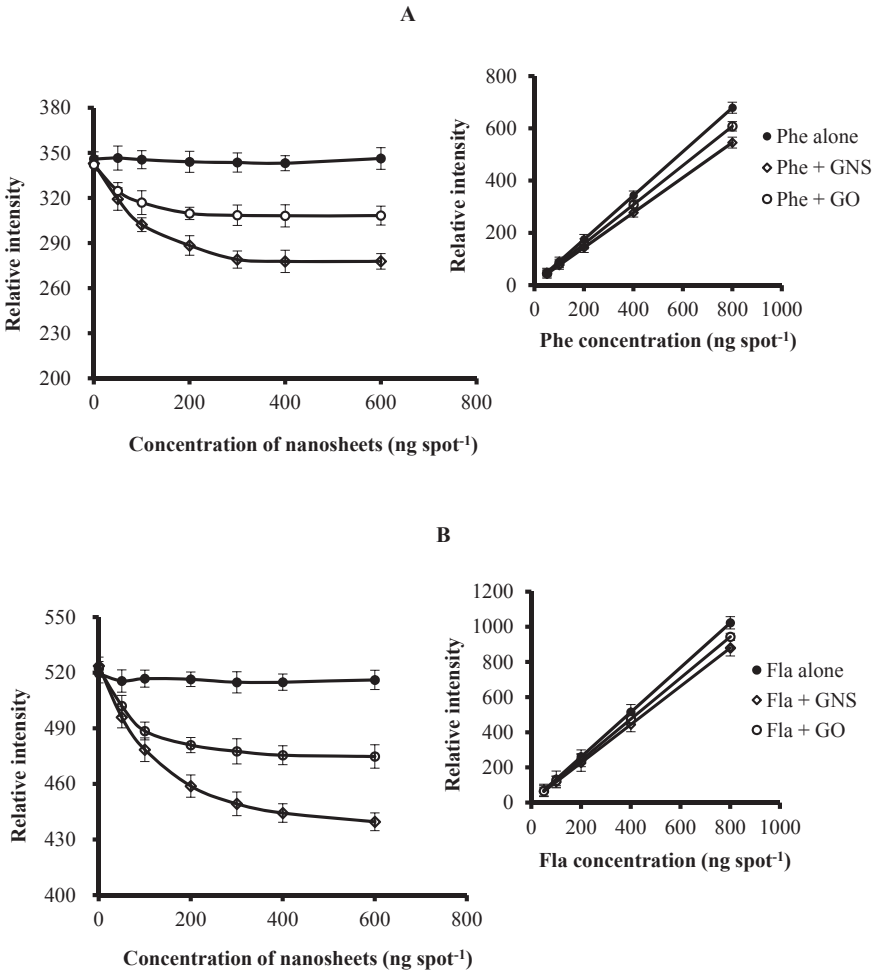

Fig. 2. Effect of GNS and GO loading on the fluorescence intensity of Phe (400 ng spot^{-1}) and Fla (400 ng spot^{-1}) and the PAH content on the fluorescence intensity in the presence of GNS (300 ng spot^{-1}) and GO (200 ng spot^{-1}).

Table 1
Analytical merits of the analytical method.

PAHs	Nanosheets		Calibration curves	Linear ranges (ng spot^{-1})	Correlation coefficients	Detection limits[c] (ng spot^{-1})
Phe	GNS (ng spot^{-1})	0	y[b] = 0.9x[a] + 7.3	4.0–950	0.9989	2.3
		100	y = 0.8x + 8.0	4.5–925	0.9953	2.6
		200	y = 0.7x + 8.8	4.8–910	0.9938	2.8
		300	y = 0.7x + 9.2	5.0–900	0.9915	3.1
		600	y = 0.6x + 9.3	5.5–895	0.9906	3.2
	GO (ng spot^{-1})	0	y = 0.9x + 7.3	4.0–950	0.9989	2.3
		100	y = 0.8x + 7.8	4.5–930	0.9962	2.5
		200	y = 0.8x + 8.1	4.7–920	0.9947	2.6
		300	y = 0.7x + 8.3	4.8–915	0.9940	2.7
		500	y = 0.7x + 8.4	5.2–910	0.9936	2.8
Fla	GNS (ng spot^{-1})	0	y = 1.3x + 6.9	3.0–960	0.9981	1.2
		100	y = 1.2x + 7.5	4.1–930	0.9964	1.5
		200	y = 1.1x + 7.9	4.5–915	0.9947	1.6
		300	y = 1.1x + 8.4	4.7–905	0.9932	1.7
		600	y = 1.0x + 8.5	5.0–895	0.9925	1.8
	GO (ng spot^{-1})	0	y = 1.3x + 6.9	3.0–960	0.9981	1.2
		100	y = 1.3x + 7.4	3.6–945	0.9954	1.4
		200	y = 1.2x + 7.6	4.0–935	0.9935	1.5
		300	y = 1.2x + 7.7	4.3–930	0.9926	1.6
		500	y = 1.1x + 7.8	4.5–920	0.9919	1.6

[a] *x* represents the concentration of PAHs adsorbed onto the living spinach surfaces.
[b] *y* represents the relative fluorescence intensity of adsorbed PAHs.
[c] Detection limits of the analytical approach, which was calculated by $3S_B/m$, where 'S_B' is the standard deviation of the blank (n = 9), and 'm' is the slope of the calibration curves.

For instance, the values decreased by 20.2% for Phe and 14.2% for Fla with GNS at a concentration of 300 ng spot^{-1}, and were decreased by 10.7% for Phe and 7.9% for Fla with GO at a concentration of 200 ng spot^{-1}. This observation could be explained by the fluorescence quenching of the two adsorbed PAHs induced by GNS and GO (Fig. S5). In published work, GNS and GO are shown to be a very efficient quencher of fluorescence molecules (Kasry et al., 2012), and Ramakrishna Matte et al. (2011) reported that the mechanism for GNS-quenching the fluorescence of aromatic molecules lies in photo-induced electron transfer. Thus, it is reasonable to extrapolate that the quenching effects observed in this study might be attributed to the electron transfer from the excited Phe and Fla to GNS and GO. Additionally, the degree of fluorescence quenching induced by GNS was about two times greater than that by GO. As reported by Kim et al. (2010), GNS has sp^2-hybridized orbitals with the same internal structure as corresponding PAHs. By inference, the coexistence of PAHs and GNS on the spinach leaf surfaces could greatly enhance the π-π interactions. Generally, the increasing π-π interactions play a crucial role in accelerating the electron or energy transfer from the sensitizer to GNS, which is bound to result in the fluorescence quenching of the adsorbed Phe and Fla. By comparison, the abundance of O-containing functional groups was markedly higher on GO than on GNS (Fig. S2), suggesting GO surface to be more highly polar. Thus, GO surface had relatively weaker π-π interactions with PAH molecules than GNS surface, which could be the logical explanation for the relatively weaker fluorescence quenching induced by GO ($p < 0.05$). In addition, for both GNS and GO, the quenching effect acting on Fla was more apparent than that on Phe, indicating that π-π interactions became much stronger between the two nanosheets and Fla relative to Phe. However, results from what have been discussed above demonstrate that the fiber-optic fluorimetry is a promising analytical platform for the *in situ* determination of the relevant levels, behavior and fates of PAHs adsorbed onto the spinach surfaces, as well as the effects of GNS and GO nanoparticles.

3.2. Depuration of PAHs adsorbed onto the spinach leaf surfaces

From Fig. S6, negligible fluctuations occurred between the sets of concentrations acquired by fiber-optic fluorimetry and GC-MS. In addition, to further evaluate the similarities of the two sets of concentrations, the value of the correlation coefficients (R^2) was calculated according to reported method (Sun et al., 2016a). The relatively good R^2 were observed for both Phe and Fla with values up to 0.9961 and 0.9975 (Fig. S6), similar results were also found for the two PAHs with other GNS and GO dosages. Therefore, the observations further confirmed the feasibility of the fiber-optic fluorimetry to accurately determine the effects of GNS and GO on the depuration of PAHs adsorbed onto spinach leaf surfaces.

As reported in our previous studies (Sun et al., 2013a, 2016b), within the same PAHs and vegetation species, the variation of PAH's initial concentrations has no influences on the depuration regularity. Similarly, a moderate initial concentration of 400 ng spot^{-1} for both Phe and Fla was chosen in the depuration experiment. Whether GNS or GO was present or not, the depuration of the two PAHs that lasting for 72 h could be split into a rapid phase (8 h) and a slow phase (64 h) under either light or dark treatment, respectively (Fig. 3 and Fig. 4). Furthermore, the disappearance of the two PAHs from the living spinach leaf surfaces was in keeping with the first-order kinetics equation (Fig. S7 and Fig. S8), which was in good agreement with the pattern observed for spruce (Niu et al., 2003), pine needles (Wang et al., 2005), mangrove (Sun et al., 2013a, 2013b) and crop species (Sun et al., 2016b). These findings further confirmed the universality of this pattern through successful application to the vegetable species.

3.2.1. Effects of GNS and GO on the rapid phase

Table 2 displays the parameters for the kinetic depuration of adsorbed Phe and Fla. Whether or not GNS or GO was present on spinach leaf surfaces, i) compared with the volatilization coefficients (k_{C1}) of dark-treated seedlings, the overall depuration coefficients (k_{T1}) of light-treated ones was slightly higher over the rapid phase; ii) the k_{C1} values was 4–8 times higher than the corresponding the photolysis coefficients (k_{P1}, deducting k_{C1} from k_{T1}). Based on these observations, it could be concluded that volatilization dominated the disappearance of adsorbed Phe and Fla from the spinach leaf surfaces during the rapid phase, further corroborating the observations derived from our published studies (Sun et al., 2013b, 2016b). Therefore, it is reasonable to extrapolate that, clarifying the effect of GNS and GO on the volatilization of the adsorbed Phe and Fla was likely sufficient to account for the overall impact on the rapid phase.

One prominent impact on the rapid phase is the changes in the kinetic parameters brought about by GNS and GO. It was noted that, as GNS and GO loadings increased, the k_{C1} values had a trend of continuous decrease that was divided into fast and slow fractions (Table 2), indicating that volatilization of the two adsorbed PAHs was inhibited. In other words, the interaction between the two nanosheets and ECW enhanced the affinity for both Phe and Fla. To date, many studies have inventoried the effects of ENMs on vascular plants (Rico et al., 2011; Peralta-Videa et al., 2011; Miralles et al., 2012). Recently, the changes in the ECW microstructure have been included as novel endpoints for the response of the exposed plants to ENM (Siddiqi and Husen, 2017). As noted in section 3.1, the addition of GNS and GO changed the polarity of the ECW, probably via altering the tortuosity or viscosity, which plays an important role in promoting the accessibility of the plant cuticle to organic compounds. On the other hand, GNS has been reported to perform good capability in the adsorption of non polar Nap, Phe and Pyr in aqueous solution, attributed to the flat surface and sieving effect of the powerful groove regions formed by wrinkles on GNS surfaces (Wang et al., 2014a; Chen and Chen, 2015). Similarly, GO has also been reported to enrich the adsorption content of individual anthracene (Ant), Pyr and benzo[a]pyrene (B[a]P) onto the *Kandelia obovata* root surface for its delocalized π-π interactions and large surface area (Tan et al., 2017). Furthermore, GNS and GO can easily be adsorbed onto the plant cell surface owing to their superior hydrophobic nature and mechanical properties (Zhao et al., 2015). All of this evidence can lead to the conclusion that the presence of GNS and GO would offer more adsorption sites and specific interaction domains for PAHs on the outer surface of spinach leaf.

Statistically, there exists significant inter-species and inter-chemical variability regarding the decreased extent of k_{C1} values ($p < 0.05$) (Table 2). As the GNS and GO loadings separately increased up to 300 ng spot^{-1}, the k_{C1} values decreased by 28.9% and 24.4%, respectively, for three-ringed Phe, and 41.9% and 31.3%, respectively, for four-ringed Fla. Wang et al. (2014b) observed that the adsorption capacity of GNS and GO for PAHs increased with the number of benzene rings of the PAH molecule. Thus, for either GNS or GO, the decreased extent of k_{C1} values characterized with Fla > Phe in this study was attributed to their greater adsorption capacity for Fla relative to Phe. Furthermore, the decreased extent of k_{C1} values with GNS was greater than that with GO. In the Raman spectra (Fig. S1), the I_D/I_G ratio of GNS (1.16) was higher than that of GO (0.83), indicating that more defects and groove regions were contained on the GNS surface. In addition, from the XPS spectra of GNS and GO (Fig. S3), the contents of O-containing moieties on GO surface, such as C-O (286.4 eV), C═O (287.5 eV), and O-C═O (289.3 eV), were markedly greater than that on GNS surface, which suggested that the GO surface was more hydrophilic than GNS, whereas the sp^2 hybridized zone on GO was much less than that of

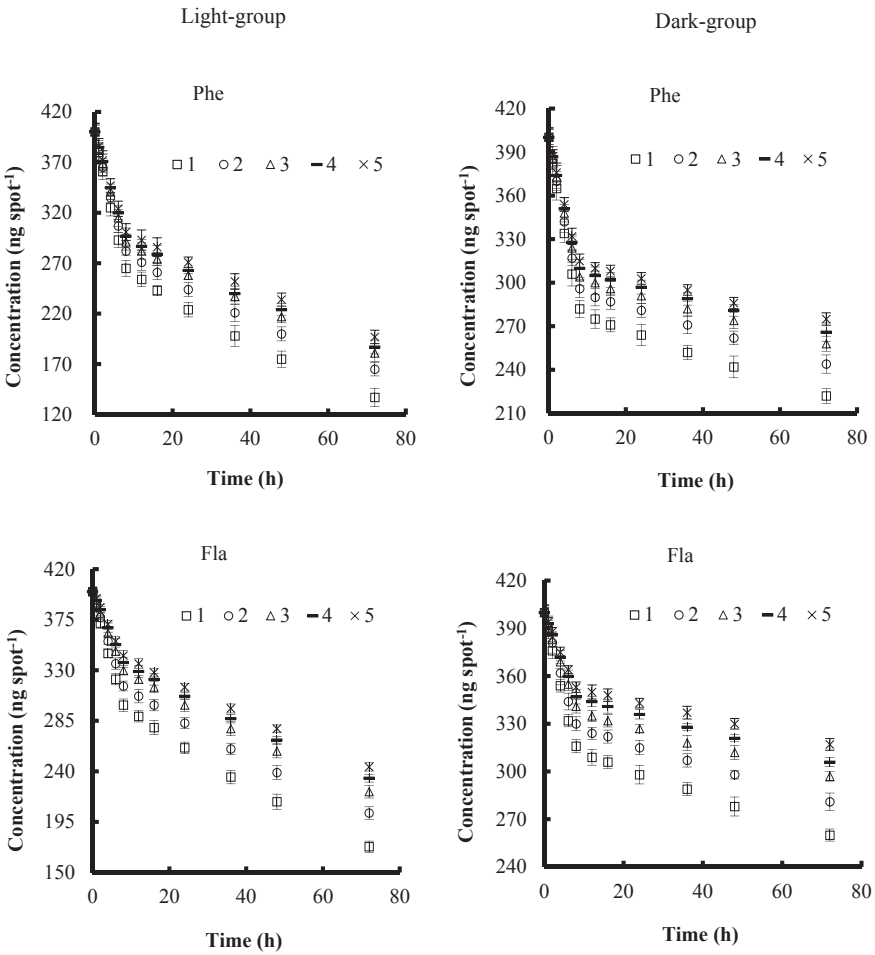

Fig. 3. Effects of GNS with different initial concentrations (1. 0; 2. 100; 3. 200; 4. 300; 5. 600 ng spot^{-1}) on the depuration of Phe and Fla adsorbed onto living spinach leaf surfaces.

GNS. Therefore, GO had relatively weaker affinity to PAHs than GNS, which could logically account for the inter-species variation in k_{C1} decreased extent. The other significant effect brought by GNS and GO on the rapid depuration process was the variations in the linearity of the decay. In the absence of GNS and GO nanosheets, the depuration of the two PAHs from the spinach leaf surfaces showed better linearity. With increasing GNS and GO concentrations, the nonlinearity of the decay curve was strengthened as R^2 values decreased (Table 2).

3.2.2. *Effects of GNS and GO on the slow phase*

During the slow phase, k_{P2} values became significantly greater than the k_{C2} values for both Phe and Fla ($p < 0.05$), especially for those with the presence of nanosheets (Table 2). Nevertheless, the k_{P2}/k_{C2} ratios ranged from 1.3 to 7.0, but were not much larger than 1, indicating that the slow depuration process was dominated by the combination of volatilization and photolysis. This finding coincided with the observation documented in our previous studies (Sun et al., 2013a, 2016b). Similar to the k_{C1} values, the k_{C2} values had a continuous decreasing trend with the increment of GNS and GO loadings. The interpretation for the decrease in k_{C2} values during the slow phase should be the same as the decrease in k_{C1} values during the rapid phase.

Similar to the k_{P1} values, the k_{P2} values decreased as the GNS loading increased, and the decreasing rate became smaller with a higher dosage of GNS, irrespective of the chemical type (Table 2). This finding suggests that the coexisting GNS nanosheets retard the photolysis of the two adsorbed PAHs. As reported, the light adsorption capacity of ECW is inversely correlated with the photolysis rate of PAHs adsorbed onto plant leaf surfaces (Sun et al., 2016b). To interpret the decrease in k_{P2} values, the UV-vis spectra of ECW isolated from the spinach seedlings were obtained following the operational procedure recorded in a previous study (Wang et al., 2008). From Fig. S9, the absorption wavelength of spinach ECW was located in the range of 270–380 nm, and the light adsorption intensity of ECW treated with GNS was higher than that without treatment ($p < 0.05$). Reasonably, the increase in the light adsorption capacities by ECW would reduce the light allocations to the PAHs adsorbed onto the spinach leaf surfaces. Consequently, the k_{P2} values of PAHs coexisting with GNS would decrease. Interestingly, the increase in the light adsorption intensity by ECW was also observed for the spinach leaves treated with GO (Fig. S9). However, the k_{P2} values of both Phe and Fla had an initial increase as GO loading escalated and then increased at a decreasing rate with GO occurrence up to higher values (Table 2). Clearly, there may be additional factors dominating the GO performance. In addition to hydroxyl, carboxyl and carbonyl groups (Fig. S1), the structure of GO contains zigzag edges and a basal plane, making GO perform good photocatalytic activities by serving as a conductor for the electron transfer during the synthesis of reactive oxygen (Wang et al., 2009; Fu and Zhu, 2013; Yu et al., 2015). Logically, the photocatalytic activities of GO accounted for the increase of the k_{P2} values. When increasing the GO dosage, the thickness of GO on the spinach leaf surfaces would increase. Since the intensity of UV light

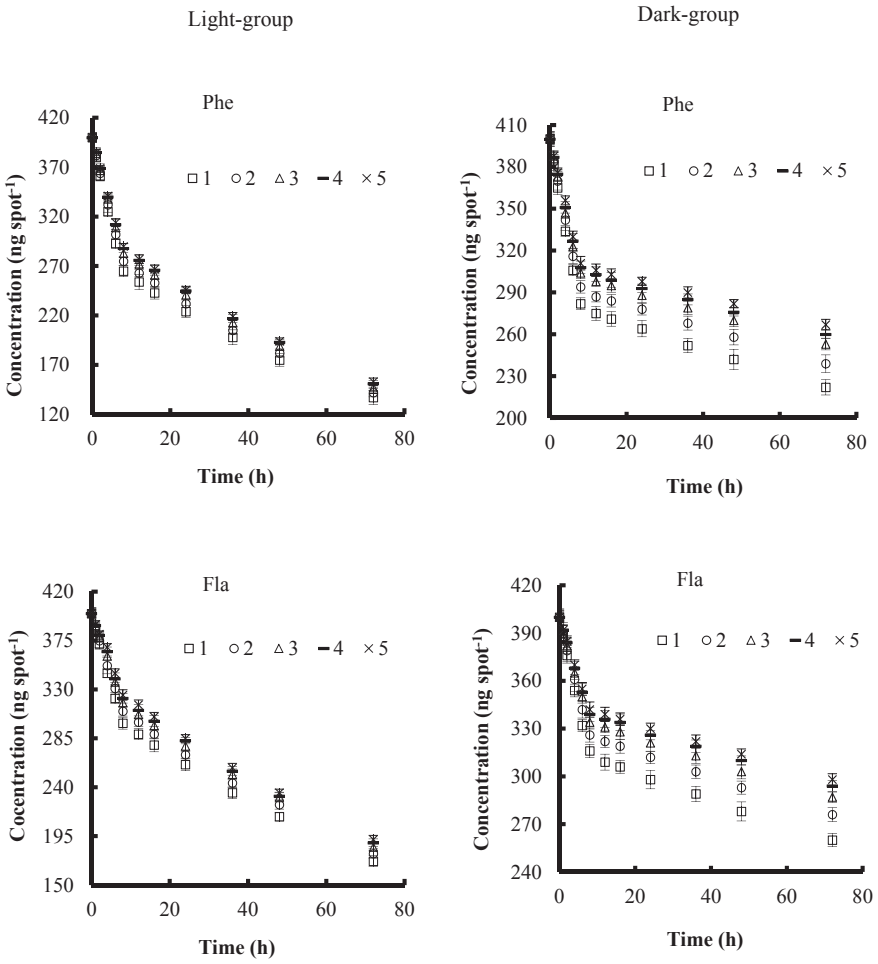

Fig. 4. Effects of GO with different initial concentrations (1. 0; 2. 100; 3. 200; 4. 300; 5. 500 ng spot^{-1}) on the depuration of Phe and Fla adsorbed onto living spinach leaf surfaces.

Table 2
Effects of GNS and GO on the kinetic parameters for the depuration of the two PAHs adsorbed onto living spinach leaf surfaces (n = 9).

PAHs	Concentration (ng spot^{-1})	Fast phase					Slow phase				
	GNS	k_{T1}(h^{-1})	R^2	k_{C1}(h^{-1})	R^2	k_{P1}	k_{T2}(h^{-1})	R^2	k_{C2}(h^{-1})	R^2	k_{P2}(h^{-1})
Phe	0	0.052	0.97	0.045	0.98	0.007	0.011	0.95	0.004	0.97	0.007
	100	0.044	0.92	0.038	0.96	0.006	0.009	0.91	0.003	0.93	0.006
	200	0.039	0.88	0.034	0.93	0.005	0.007	0.86	0.002	0.90	0.005
	300	0.037	0.85	0.032	0.92	0.005	0.007	0.82	0.002	0.86	0.005
	600	0.035	0.82	0.031	0.89	0.004	0.005	0.79	0.001	0.82	0.004
Fla	0	0.036	0.97	0.031	0.97	0.006	0.009	0.94	0.003	0.98	0.006
	100	0.029	0.93	0.024	0.94	0.005	0.007	0.92	0.002	0.95	0.005
	200	0.024	0.90	0.020	0.88	0.004	0.006	0.88	0.002	0.91	0.004
	300	0.022	0.87	0.018	0.90	0.004	0.005	0.85	0.002	0.87	0.003
	600	0.018	0.84	0.015	0.85	0.003	0.004	0.80	0.001	0.83	0.003
	GO										
Phe	0	0.052	0.95	0.045	0.98	0.007	0.011	0.96	0.005	0.97	0.006
	100	0.047	0.91	0.040	0.92	0.007	0.010	0.94	0.003	0.89	0.007
	200	0.044	0.86	0.036	0.89	0.008	0.010	0.93	0.002	0.91	0.008
	300	0.043	0.84	0.034	0.83	0.009	0.010	0.91	0.002	0.85	0.008
	500	0.042	0.81	0.033	0.88	0.009	0.009	0.90	0.001	0.83	0.008
Fla	0	0.037	0.96	0.032	0.97	0.005	0.009	0.98	0.004	0.98	0.005
	100	0.033	0.91	0.027	0.92	0.006	0.009	0.90	0.003	0.93	0.006
	200	0.031	0.89	0.024	0.85	0.007	0.008	0.83	0.001	0.85	0.007
	300	0.029	0.84	0.022	0.82	0.007	0.008	0.85	0.001	0.87	0.007
	500	0.029	0.86	0.021	0.81	0.008	0.008	0.87	0.001	0.82	0.007

k_{T1} and k_{T2} represent the total depuration coefficients of adsorbed PAHs over the rapid and slow phase, respectively; k_{C1} and k_{C2} represent the volatilization coefficients of PAHs over the rapid and slow phase, respectively; k_{P1} and k_{P2} represent the photolysis coefficients of PAHs over the rapid and slow phase, respectively.

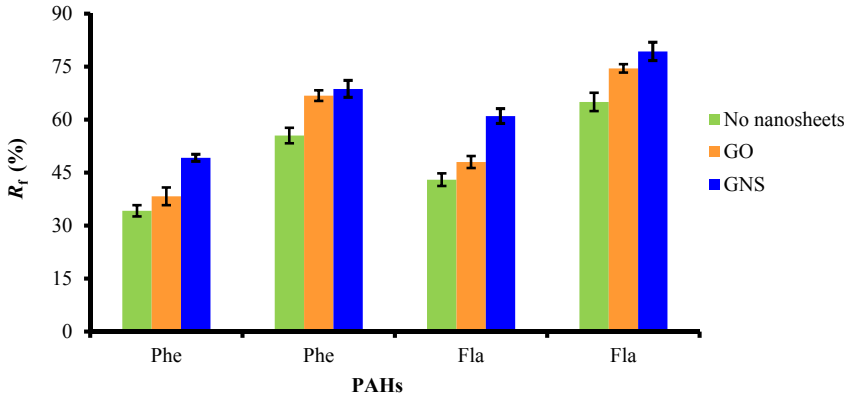

Fig. 5. Effects of GNS (600 ng spot^{-1}) and GO (500 ng spot^{-1}) on the percentage final residues of Phe and Fla on living spinach leaf surfaces.

decays rapidly with thickening of the solid phase (Wang et al., 2009), the UV light utilization rate would decrease for PAH degradation with an increased concentration of GO. Consequently, photocatalytic activities became relatively weaker with the increase in GO dosage. Finally, when GNS or GO was present at a certain level, the decay curves of both Phe and Fla showed more nonlinearity during the slow phase than during the fast phase (Table 2), owing to the assignable influence of GNS or GO on photolysis during the slow phase.

3.2.3. *Impact of GNS and GO on PAH residues*

Through the discussion above, the GNS and GO affected the depuration of PAHs from the living spinach leaf surfaces mainly by altering volatilization and photolysis processes. Furthermore, the effects of the two nanosheets on vegetable security remain to be evaluated. From Fig. 5, regardless of the light- or dark-treated seedlings, the percentage of final residues (R_f) of either Phe or Fla remaining on living spinach leaf surfaces with GNS at the highest concentration of 600 ng spot^{-1} was significantly greater than that without the nanosheets ($p < 0.05$). The increment of R_f values for the dark-treated group further confirmed the inhibition effect of GNS on the volatilization of adsorbed Phe and Fla; for the light-treated ones, comparably greater R_f values were attributed to the inhibition effect of GNS on both volatilization and photolysis. Similarly, the R_f values of the two PAHs with GO at the highest concentration of 500 ng spot^{-1} was also larger than that without GO nanosheets (Fig. 5). The increase of R_f values for the dark-treated spinach could also be explained by GO-induced inhibition to volatilization. However for light-treated plants, the reason for the increase of R_f values was that the inhibitory effect of GO on volatilization exceeded its promoting effect on photolysis. In short, the addition of GNS and GO increased the accumulation of PAHs on the spinach leaf surfaces to varying degrees, potentially threatening vegetable security and public health via the dietary pathway.

4. Conclusion

The established fiber-optic fluorimetry not only shows high potential for *in situ* quantification of PAHs adsorbed onto the vegetable leaf surfaces, but also has excellent applicability for examining the impact of GNS and GO on the depuration of the adsorbed PAHs. In summary, the impact on the depuration are mainly embodied in the variation of spectral features, volatilization and photolysis processes of the adsorbed PAHs, a finding that is closely associated with the types and dosages of nanosheets. For each PAH chemical, volatilization was diminished to different extents when GNS and GO were separately present. The photolysis was inhibited by GNS because its occurrence reduced the solar irradiation that acting on PAHs' degradation through the increase in light adsorption ability of ECW. By contrast, the photocatalytic activity by GO promoted the photolysis of the adsorbed PAHs. Overall, the presence of the two types of nanosheets inhibited the total depuration of PAHs from the living spinach leaf surfaces. The impact of nanosheets on the potential risk associated with edible vegetable contamination by PAHs is an active investigation and a subject of concern.

Acknowledgments

The authors would like to thank the financial support from the Natural Science Foundation of China (Nos. 21507077, 91543203 and 41501563), Shanxi Province Science Foundation for Youths (201601D021131), Guangzhou Key Laboratory of Environmental Exposure and Health (No. GZKLEEH201609), a grant from the Central Promotion Plan of Talent Development (rsc801), andResearch Project for Young Sanjin Scholarship of Shanxi, Program for the Outstanding Innovative Teams of Higher Learning Institutions of Shanxi.

Appendix A. Supplementary data

Supplementary data related to this article can be found at https://doi.org/10.1016/j.envpol.2017.11.007.

References

Andersson, J.T., Achten, C., 2015. Time to say goodbye to the 16 EPA PAHs? Toward an upto date use of PACs for environmental purposes. Polycycl. Aromat. Compd. 35 (2–4), 330–334.

Corredor, E., Testillano, P.S., Coronado, M.J., Gonzalez-Melendi, P., Fernandez-Pacheco, R., Marquina, C., Ibarra, M.R., de la Fuente, J.M., Rubiales, D., Perez-de-Luque, A., Risueno, M.C., 2009. Nanoparticle penetration and transport in living pumpkin plants: *In situ* subcellular identification. BMC Plant Biol. 9, 45–46.

Chen, L., Zhang, Y., Liu, B.B., 2010. *In situ* simultaneous determination the photolysis of multi-component PAHs adsorbed on the leaf surfaces of living *Kandelia candel* seedlings. Talanta 83, 324–331.

Chen, X.X., Chen, B.L., 2015. Macroscopic and spectroscopic investigations of the adsorption of nitro aromatic compounds on graphene oxide, reduced graphene oxide, and graphene nanosheets. Environ. Sci. Technol. 49, 6181–6189.

De La Torre-Roche, R., Hawthorne, J., Deng, Y.Q., Xing, B.S., Cai, W.J., Newman, L.A., Wang, C., Ma, X.M., White, J.C., 2012. Fullerene-enhanced accumulation of *p,p′*-DDE in agricultural crop species. Environ. Sci. Technol. 46, 9315–9323.

De La Torre-Roche, R., Hawthorne, J., Musante, C., Xing, B.S., Newman, L.A., Ma, X.M., White, J.C., 2013. Impact of Ag nanoparticle exposure on *p,p′*-DDE bioaccumulation by *cucurbita pepo* (zucchini) and *glycine max* (soybean). Environ. Sci. Technol. 47, 718–725.

Fu, H.Y., Zhu, D.Q., 2013. Graphene oxide-facilitated reduction of nitrobenzene in sulfide-containing aquesous solution. Environ. Sci. Technol. 47, 4204–4210.

Geim, A.K., Novoselov, K.S., 2007. The rise of graphene. Nat. Mater. 6, 183–191.

Kasry, A., Ardakani, A.A., Tulevski, G.S., Menges, B., Copel, M., Vyklicky, L., 2012. Highly efficient fluorescence quenching with graphene. J. Phys. Chem. C 116, 2858–2862.
Khillare, P.S., Jyethi, D.S., Sarkar, S., 2012. Health risk assessment of polycyclic aromatic hydrocarbons and heavy metals via dietary intake of vegetables grown in the vicintiy of thermal power plants. Food Chem. Toxicol. 50, 1642–1652.
Kim, J., Cote, L.J., Kim, F., Yuan, W., Shull, K.R., Huang, J., 2010. Graphene oxide sheets at interfaces. J. Am. Chem. Soc. 132, 8180–8186.
Li, Y.G., Chen, B.L., 2009. Phenanthrene sorption by fruit cuticles and potato peridern with different compositional characteristics. J. Agric. Food Chem. 57, 637–644.
Li, Y.G., Chen, B.L., Chen, Z.M., Zhu, L.Z., 2009. Surfactant effects on the affinity of plant cuticles with organic pollutants. J. Agric. Food Chem. 57, 3681–3688.
Maliyekkal, S.M., Sreeprasad, T.S., Krishnan, D., Kouser, S., Mishra, A.K., Waghmare, U.V., Pradeep, T., 2013. Graphene: a reusable substrate for unprecedented adsorption of pesticides. Small 9, 273–283.
Miralles, P., Church, T.L., Harris, A.T., 2012. Toxicity, uptake, and translocation of engineered nanomaterials in vascular plants. Environ. Sci. Technol. 46, 9224–9239.
Mitrano, D.M., Motellier, S., Clavaguera, S., Nowack, B., 2015. Review of nanomaterial aging and transformation through the life cycle of nano-enhanced products. Environ. Int. 77, 132–147.
Mueller, T., Xia, F.N., Avouris, P., 2010. Graphene photodetections for high-speed optical communications. Nat. Photonics 6, 297–301.
Niu, J.F., Chen, J.W., Martens, D., Quan, X., Yang, F.L., Kettrup, A., Schramm, K.-W., 2003. Photolysis of polycyclic aromatic hydrocarbons adsorbed on spruce [*Piceaabies* (L.) Karst.] needles under sunlight irradiation. Environ. Pollut. 123, 39–45.
Nizzetto, L., Liu, X., Zhang, G., Komprdova, K., Komprda, J., 2014. Accumulation kinetics and equilibrium partitioning coefficients for semivolatile organic pollutants in forest litter. Environ. Sci. Technol. 48, 420–428.
Peralta-Videa, J.R., Zhao, L., Lopez-Moreno, M.L., de la Rosa, G., Hong, J., Gardea-Torresdey, J.L., 2011. Nanomaterials and the environment: a review for the biennium 2008-2010. J. Hazard. Mater 186, 1–15.
Ramakrishna Matte, H.S.S., Subrahmanyam, K.S., VenkataRao, K., George, S.J., Rao, C.N.R., 2011. Quenching of fluorescence of aromatic molecules by graphene. Chem. Phys. Lett. 506, 260–264.
Rico, C.M., Majumdar, S., Duarte-Gardea, M., Peralta-Videa, J.R., Gardea-Torresdey, J.L., 2011. Interaction of nanoparticles with edible plants and their possible implications in the food chain. J. Agric. Food Chem. 59, 3485–3498.
Siddiqi, K.S., Husen, A., 2017. Plant response to engineered metal oxide nanoparticles. Nanoscale Res. Lett. 12, 92.
Smith, K.E.C., Thomas, G.O., Jones, K.C., 2001. Seasonal and species differences in the air-pasture transfer of PAHs. Environ. Sci. Technol. 35, 2156–2165.
Sun, H.F., Guo, S., Zhu, N., Sang, N., Chen, Z., 2016a. *In situ* determination of multiple polycyclic aromatic hydrocarbons uptake by crop leaf surfaces using multi-way models. Environ. Pollut. 218, 523–529.
Sun, H.F., Li, R.L., Zhu, Y.X., Zhang, Y., 2013a. *In situ* determination mechanisms for the depuration of polycyclic aromatic hydrocarbons adsorbed onto the leaf surfaces of living mangrove seedlings. J. Hazard. Mater 262, 339–347.
Sun, H.F., Wang, W.P., Guo, S., Zhang, Y., 2016b. *In situ* investigation into surfactant effects on the clearance of polycyclic aromatic hydrocarbons adsorbed onto soybean leaf surfaces. Environ. Pollut. 210, 330–337.
Sun, H.F., Yang, Y.N., Zhu, Y.X., Zhang, Y., 2013b. *In situ* investigation of the depuration of fluoranthene adsorbed on the leaf surfaces of living mangrove seedlings. Talanta 116, 441–447.
Tan, H.D., Li, R.L., Zhu, Y.X., Zhang, Y., 2017. *In situ* quantitative and visual investigation of the retention of polycyclic aromatic hydrocarbons on the root surface of *Kandelia obovata* using a microscopic fluorescence spectral analysis method. Talanta 167, 86–93.
Trujillo-Cayado, L.A., Garcia, M.C., Santos, J., Carmona, J.A., Alfaro, M.C., 2017. Progress in the formulation of concentrated ecological emulsions for agrochemcial application based on environmentally friendly ingredients. ACS Sustain. Chem. Eng. 5, 4127–4132.
Wang, D.G., Chen, J.W., Xu, Z., Qiao, X.L., Huang, L.P., 2005. Disappearance of polycyclic aromatic hydrocarbons sorbed on surfaces of pine [*Pinuathunbergii*] needles under irradiation of sunlight: volatilization and photolysis. Atmos. Environ. 39, 4583–4591.
Wang, F.F., Wang, F., Zhu, D.Q., Chen, W., 2015. Effects of sulfide reduction on adsorption affinities of colloidal graphene oxide nanoparticles for phenanthrene and 1-naphthol. Environ. Pollut. 196, 371–378.
Wang, J., Chen, B.L., Xing, B.S., 2016. Wrinkles and folds of activated graphene nanosheets as fast and efficient adsorptive sites for hydrophobic organic contaminants. Environ. Sci. Technol. 50, 3798–3808.
Wang, J., Chen, Z.M., Chen, B.L., 2014a. Adsorption of polycyclic aromatic hydrocarbons by graphene and graphene oxide nanosheets. Environ. Sci. Technol. 48, 4817–4825.
Wang, Y., Liu, C.S., Li, F.B., Liu, C.P., Liang, J.B., 2009. Photodegradation of polycyclic aromatic hydrocarbon pyrene by rion oxide in solid phase. J. Hazard. Mater 162, 716–723.
Wang, Y.F., Wu, Y., Pi, N., Tam, N.F.Y., 2014b. Investigation of microbial community structure in constructed mangrove microcosms receiving waster-borne polycyclic aromatic hydrocarbons (PAHs) and polybrominated diphenyl ethers (PBDEs). Environ. Pollut. 187, 136–144.
Wang, Y.Q., Tao, S., Jiao, X.C., Covney, R.M., Wu, S.P., Xing, B.S., 2008. Polycyclic aromatic hydrocarbons in leaf cuticles and inner tissues of six species of trees in urban Beijing. Environ. Pollut. 151, 158–164.
Yu, J.G., Yu, L.Y., Yang, H., Liu, Q., Chen, X.H., Jiang, X.Y., Chen, X.Q., Jiao, F.P., 2015. Graphene nanosheets as novel adsorbents in adsorption, preconcentration and removal of gases, organic compounds and metal ions. Sci. Total Environ. 502, 70–79.
Yu, S.J., Wang, X.X., Yao, W., Wang, J., Ji, Y.F., Ai, Y.J., Alsaedi, A., Hayat, T., Wang, X.K., 2017. Macroscopic, spectroscopic, and theoretical investigation for the interaction of phenol and naphthol on reduced graphene oxide. Environ. Sci. Technol. 51, 3278–3286.
Zhang, P., Ma, Y.H., Liu, S.T., Wang, G.H., Zhang, J.Z., He, X., Zhang, J., Rui, Y.K., Zhang, Z.Y., 2017. Photoxicity, uptake and transformation of nano-CeO_2 in sand cultured romain lettuce. Environ. Pollut. 220, 1400–1408.
Zhao, S.Q., Wang, Q.Q., Zhao, Y.L., Rui, Q., Wang, D.Y., 2015. Toxicity and translocation of graphene oxide in *Arabidopsis thanliana*. Environ. Toxicol. Phar 39, 145–156.